Hindawi
Journal of Nanomaterials
Volume 2018, Article ID 3498527, 9 pages
https://doi.org/10.1155/2018/3498527

Research Article

Antifungal Activity of ZnO and MgO Nanomaterials and Their Mixtures against *Colletotrichum gloeosporioides* Strains from Tropical Fruit

Susana C. De la Rosa-García,[1] **Pablo Martínez-Torres**,[2] **Sergio Gómez-Cornelio**,[3] **Mario Alberto Corral-Aguado**,[2] **Patricia Quintana**,[4] **and Nikte M. Gómez-Ortíz**[2]

[1]*Laboratorio de Microbiología Aplicada, División Académica de Ciencias Biológicas, Universidad Juárez Autónoma de Tabasco (UJAT), CP 86150 Villahermosa, TAB, Mexico*
[2]*Instituto de Física y Matemáticas, Universidad Michoacana de San Nicolás de Hidalgo, Ciudad Universitaria, CP 58040 Morelia, MICH, Mexico*
[3]*Universidad Politécnica del Centro, Carretera Federal Villahermosa-Teapa, Km. 22.5, 86290 Tumbulushal, Centro, TAB, Mexico*
[4]*Física Aplicada, CINVESTAV-IPN, A.P. 73, Cordemex, 97310 Mérida, YUC, Mexico*

Correspondence should be addressed to Nikte M. Gómez-Ortíz; nikte.m.g.o@gmail.com

Received 16 February 2018; Accepted 18 April 2018; Published 19 August 2018

Academic Editor: Surinder Singh

Avocado (*Persea americana*) and papaya (*Carica papaya*) are tropical fruits with high international demand. However, these commercially important crops are affected by the fungus *Colletotrichum gloeosporioides*, which causes anthracnose and results in significant economic losses. The antifungal activity of metal oxide nanomaterials (zinc oxide (ZnO), magnesium oxide (MgO), and ZnO:MgO and ZnO:$Mg(OH)_2$ composites) prepared under different conditions of synthesis was evaluated against strains of *C. gloeosporioides* obtained from papaya and avocado. All nanoparticles (NPs) at the tested concentrations significantly inhibited the germination of conidia and caused structural damage to the fungal cells. According to the radial growth test, the fungal strain obtained from avocado was more susceptible to the NPs than the strain obtained from papaya. The effect of the tested NPs on the fungal strains confirmed that these NPs could be used as strong antifungal agents against *C. gloeosporioides* to control anthracnose in tropical fruits.

1. Introduction

Colletotrichum gloeosporioides is a phytopathogenic agent that causes anthracnose disease in several fruits and crops, including avocado, papaya, mango, pitaya, tomatoes, citrus, and almonds, among others [1–3]. The anthracnose pathogen invades the leaves, flowers, and fruits during preharvest and also invades postharvest fresh products [4]. The severity of the disease is related with environmental conditions. The most severe attacks on fruits or crops occur when crops are most susceptible (e.g., during flowering and/or fruiting) and under conditions of high humidity (e.g., during the rainy season). Meanwhile, the fungus is inactive under dry climate conditions, sunlight, and extreme temperatures [3].

The symptoms of anthracnose depend on the affected plant and its physiology. The symptoms of anthracnose in papaya (*Carica papaya* L.) include sunken spots of different colors on the leaves and necrosis on the stems, fruits, or flowers, which often result in the wilting or death of plant tissues. In avocado (*Persea americana*), the fungus mainly infects small fruits growing in orchards; conidia are deposited on small fruits, germinate, and form appressoria. Anthracnose does not fully develop until fruits mature yet eventually results in the appearance of sunken necrotic black spots [5].

Synthetic fungicides are used to protect harvests from such fungal diseases. However, these can potentially contaminate soils and water and can present potential risks for

Table 1: Methods of synthesis of different metal oxide nanomaterials.

Material	Method of synthesis	Sample	Temperature of synthesis (°C)	Hydrothermal treatment (°C)/time (h)	Calcination (°C)
MgO	Coprecipitation	S1	70	—	500
		S2	70	—	1000
ZnO	Coprecipitation	S3	25	—	500
		S4	70	—	1000
	Hydrothermal	S5	25	100/24	—
		S6	25	160/24	—
$ZnO/Mg(OH)_2$	Hydrothermal	S7	25	100/24	—
		S8	25	160/24	—
		S9	70	100/24	—
		S10	70	160/24	—
ZnO/MgO	Coprecipitation	S11	25	—	500
		S12	70	—	500
		S13	70	—	1000

human and animal health [6]. Furthermore, fungi have developed resistance to several commercial fungicides [7], resulting in important economic losses. This problem has led to the search of new technologies and antimicrobial agents, such as nanomaterials, to control fungal infections in crops.

Currently, nanotechnology could have the potential to revolutionize the agriculture and food industry, to provide new tools to treat phytopathogenic diseases, and to enhance the ability of plants to absorb nutrients [8]. Several nanomaterials have been shown to have antifungal properties like silver [9, 10], copper [11, 12], zincite [13, 14], titania [15], nickel, and core-shell Ag-SiO_2 [16]. The nanoparticles (NPs) may be good candidates as fungicides in crops, by their unique physical and chemical properties, which often differ significantly from their bulk properties [17, 18]. For example, the size of NPs affects the optical, catalytic, and electronic properties of these materials [19, 20] that can provide different antifungal effects.

In particular, inorganic metal oxides such as MgO and ZnO have attracted interest as antimicrobial agents because of their safety and stability [21]. However, several physical and chemical methods are used for the synthesis of NPs and may provide nanoparticles of different morphologies and sizes. In this work, we synthesized ZnO powder using both coprecipitation and hydrothermal methods, while the MgO powder was only prepared by coprecipitation. We got ZnO and MgO nanoparticles with different sizes and morphologies and determined their antifungal properties against the causal agent of anthracnose, *C. gloeosporioides* isolated from avocado leaves and papaya fruits.

2. Materials and Methods

2.1. Synthesis of Metal Oxides

2.1.1. Synthesis of Metal Oxides by Coprecipitation Method. Zinc and magnesium nitrate hexahydrate (denoted as $X(NO_3)\cdot 6H_2O$ with X = Zn or Mg) were used as precursors to obtain ZnO and MgO NPs, and sodium hydroxide (NaOH) was used as a precipitating agent.

Specifically, the coprecipitation of ZnO and MgO was performed following the method of Tamilsevi [22]. Briefly, the NPs were synthesized as follows: a solution of 0.4 M NaOH (Aldrich, 98%) was added drop by drop to a solution of 0.2 M $X(NO_3)\cdot 6H_2O$ (Aldrich, 98%) under constant stirring at two different temperatures of synthesis (25°C and 70°C).

To formulate the ZnO/MgO composites, a mixture of 0.2 M $Zn(NO_3)\cdot 6H_2O$ and $Mg(NO_3)\cdot 6H_2O$ (1 : 1) was reacted with 0.8 M NaOH drop by drop under constant stirring at two different temperatures of synthesis (25°C and 70°C).

2.1.2. Synthesis of Metal Oxides by Hydrothermal Method. The hydrothermal synthesis of ZnO NPs was also performed as follows: 100 mL of 0.2 M $Zn(NO_3)\cdot 6H_2O$ water solution was added drop by drop to 100 mL of 0.4 M NaOH (Aldrich, 98%) under constant stirring. This reaction was hydrothermally treated in a Teflon cup enclosed in a stainless steel pressure vessel (Parr, 4749). The hydrothermal treatments were carried out at temperatures of 100°C and 160°C for 24 h to modify and control the average particle size.

To formulate the $ZnO/Mg(OH)_2$ composites, a mixture of 0.2 M $Zn(NO_3)\cdot 6H_2O$ and $Mg(NO_3)\cdot 6H_2O$ (1 : 1) was reacted with 0.8 M NaOH drop by drop under constant stirring at two different temperatures of synthesis (25°C and 70°C). The reaction was hydrothermally treated at 100°C or 160°C for 24 h.

Following the methods described above, all samples were centrifuged and washed using distilled water (18 MΩ·cm) and ethanol (1 : 1), and the resultant precipitates were dried at 50°C. The samples obtained by the coprecipitation method were calcined in a programmable muffle furnace at 500°C or 1000°C with a constant heating rate of 5°C/min and a 2 h dwell time.

The main features of the methods used to synthesize these nanomaterials are presented in Table 1.

2.2. Characterization of Nanoparticles. The phase composition of the oxide NPs was analyzed by X-ray diffraction (XRD, D5000 Siemens) with Bragg-Brentano geometry and Cu-Kα radiation ($\lambda = 1.5418$ Å) under the following scan parameters: step size = 0.02°, $t = 5$ s, and $20^\circ \leq 2\theta \leq 80^\circ$. The phase analysis of the materials was carried out before the antifungal evaluation. The crystallite size, r, was also calculated using the Scherrer equation:

$$r = \frac{0.9\lambda}{2B\cos\theta}, \quad (1)$$

where λ is the wavelength of the radiation source, θ is the angle of reflection, and B is the peak width (FWHM; in radians) corrected for instrument broadening and determined from the spectra of large crystallites of the same materials ($B_{\text{ins}} = 2.9 \times 10^{-3}$rad).

Scanning electron microscopy (SEM, JEOL JSM-7600F) was used to determine the morphology and size of the NPs. To collect SEM images, the nanomaterials were suspended in deionized water and ultrasonicated for about 10 min. Then, a drop of this solution was deposited onto graphite paper, and the images were taken.

2.3. Isolation and Identification of Strains Caused by Anthracnose. Fungi were isolated from avocado leaves (*Persea americana*) and papaya fruits (*Carica papaya*) with characteristics symptoms of anthracnose from the states of Michoacan and Campeche, Mexico, respectively.

Tiny black spots of papaya fruit were incubated at 28°C for three days in a humidity chamber to increase the infected areas. Avocado leaves with lesions typical of anthracnose were washed in running tap water and surface sterilized by immersing and agitating in 70% ethanol for 1 min and in 0.5% sodium hypochlorite solution for 5 min followed by 3 washes in sterile distilled water for 5 min each.

The black spots on papaya fruits and avocado leaves were removed (1×1 cm^2) using a sterile scalpel and deposited onto potato dextrose agar (PDA, Difco) amended with chloramphenicol (50 μg/L) to suppress bacterial growth. The samples were incubated at 25°C for 10–15 days. The fungal hyphal tips growing in this prior culture were then transferred to fresh PDA without antibiotic and incubated again.

The isolated strains were identified by their micro- and macroscopic morphologies as *Colletotrichum gloeosporioides* according to Sutton and Weir et al. [23, 24].

2.4. Assay of Pathogenic Activity and Profiles of Susceptibility. All isolates were conducted to pathogenicity tests. Koch's postulates were used to confirm anthracnose on avocado and papaya fruits, and the fungal strains were labeled as AP-14 and PG-16, respectively. Fruits were evaluated by the presence or absence of lesions, and diseased fruits were submitted to reisolation to confirm the presence of the pathogen in infected tissues and completed by the Koch's Postulates.

The profile of susceptibility of both strains of *C. gloeosporioides* was evaluated with different commercial fungicides commonly used to prevent and control anthracnose in orchards for comparing with the synthesized NPs.

The commercial fungicides were prochloraz (Mirage® 40 EC (1-[N-propyl-N-[2-(2,4,6-trichlorophenoxy)ethyl]carbomoyl]imidazole) ADAMA, Chile) and benomyl (Benomyl 50 pH Antrak® (methyl 1-(butylcarbamoyl)benzimidazol-2-yl-carbamate) Agroquímica Tridente, Mexico) at concentrations of 1000, 100, 10, and 1 μg/mL.

2.5. In Vitro Antifungal Assay

2.5.1. Broth Microdilution Method. The *C. gloeosporioides* inocula of both strains were grown on PDA plates at 28°C for 5–10 days. Fungal growth from the plates was flooded with sterile saline solution (0.85%) and gently scraped with a sterile slide. Under aseptic conditions, the conidial suspensions were filtered through sterile gauze to remove mycelia. The number of conidia in the filtered material was counted in a Neubauer chamber and adjusted to a final concentration of 1×10^6 conidia/mL by adding potato dextrose broth (PDB, Difco).

The *in vitro* antifungal activity was determined by calculating the minimum inhibitory concentrations (MICs) of the synthesized nanomaterials [25] using microdilution methods in culture broth, following the M38-A2 protocol of the Clinical and Laboratory Standards Institute® (CLSI). All NPs were dissolved in DMSO (dimethyl sulfoxide) and diluted in sterile 96-well plates (Nunc F96 microtiter plates) with PDB in a geometric progression from 2 to 2048 times. Thus, the wells contained 100 μL of PDB with different concentrations of NPs in serial 2-fold dilutions (5, 2.5, 1.25, 0.625, 0.312, 0.156, 0.078, 0.039, 0.019, 0.009, 0.004, and 0.002 mg/mL). After the NPs were diluted, 100 μL suspensions of 1×10^5 conidia/mL were inoculated. Prochloraz was used as the positive control and DMSO as the negative control. The assays were performed in triplicate and were incubated for 48 h at 28°C. The MIC endpoint criterion for each fungus was defined as the lowest concentration of fungal growth and was determined visually by optical microscopy.

The fungicidal activity was then determined by calculating the minimum fungicidal concentration (MFC) of the NPs with fungicidal or fungistatic action. A fungicidal agent kills cells at concentrations similar to its MIC. Conversely, a fungistatic compound may be unable to kill all fungal cells despite having a strong MIC. After the MIC measurements, the MFCs were established by taking 5 μL of each well with no visible fungal growth and inoculating it on a fresh PDA medium. After incubation for 72 h at 28°C, the number of surviving organisms was determined. The MFC was defined as the lowest concentration at which 99.9% of the fungus was killed.

2.5.2. Effect of Nanoparticles on Mycelial Radial Growth. The effect of the synthesized nanomaterials on the inhibition of the mycelial growth of the two evaluated strains of *C. gloeosporioides* was also determined. The evaluated treatments were as follows: (1) culture medium without treatment (negative control), (2) culture media with two commercial fungicides (positive controls), and (3) culture media with

three MICs of NPs (0.625, 0.312, and 0.156 mg/mL) according to the broth microdilution assay.

The evaluated NP concentrations were added to culture media that were cooled to 50°C prior to being placed in Petri dishes (90 mm diameter × 15 mm thick). One day later, the center of each dish was inoculated with an agar disk (6 mm diameter) bearing mycelial growth from an 8-day-old *C. gloeosporioides* culture. The experiment was carried out in triplicate and incubated at 28°C for nine days. The radial inhibition rate was calculated when the mycelial growth of the control plate reached the edge of the Petri dish using the equation $(R - r)/R \times 100\,(\%)$ [26], where R is the radial growth of the fungal mycelia on the control plate and r is the radial growth of fungal mycelia on plates treated with NPs or commercial fungicides. From these assays, slides were prepared to analyze the structural damage to fungi resulting from the NPs via optical microscopy (Carl Zeiss, Germany) and atomic force microscopy (AFM, NT-MDT-NTEGRA Prima, Russia). The AFM images were captured under ambient conditions (RH = 45%, $T = 25$°C) using a R-TESPA probe (Bruker) in semicontact mode with a spring constant of $k = 40$ N/m at a scanning rate of 0.7 Hz. The images were analyzed in the NOVA 1.1.0.1921 software.

3. Results and Discussion

3.1. Characterization of Metal Oxide Nanomaterials. Figure 1 shows a representative XRD patterns for all synthetized nanomaterials described in Table 1. S2, S4, S6, S10, and S12 correspond to MgO by coprecipitation, ZnO by coprecipitation, ZnO by hydrothermal, ZnO/$Mg(OH)_2$ composite by hydrothermal, and ZnO/MgO composite by coprecipitation, respectively. The XRD data indicate the high crystallinity of all samples. The structural phase of MgO was periclase (S1, S2; Table 1). The ZnO synthesized by both the coprecipitation and the hydrothermal methods had the same XRD pattern corresponding to zincite (S3, S4, S5, and S6; Table 1). Their diffraction patterns only differed in terms of the width of peaks, which is related with the size of crystallites (Table 2). The ZnO/MgO composite presented the diffraction peaks of both phases of zincite and periclase (S11, S12, and S13; Table 1). The XRD of ZnO/$Mg(OH)_2$ composite presented the diffraction peaks of zincite and brucite ($Mg(OH)_2$) phases (S7, S8, S9, and S10; Table 1).

The SEM images of the synthesized materials S1 and S2 (Figure 2) correspond with MgO calcined at 500°C and 1000°C, respectively; these two materials have layers with flake morphology. Samples S3 and S4 correspond with ZnO calcined at 500°C and 1000°C, respectively, via coprecipitation method. Small spheres and some cylinders can be observed in S3, whereas S4 exhibits well-defined hexagonal bars. Meanwhile, in the hydrothermal synthesis of ZnO, some hexagonal bars and ovoid structures are observed in S5; in addition, S6 shows some prisms with pyramidal ends. ZnO/$Mg(OH)_2$ composite (S7–S10), amorphous flakes and some bars are observed. Finally, ZnO/MgO composites (S11, S12, and S13) show aggregates of amorphous flakes. S11 is not presented because it had the same morphology, crystallite, and particle size with the sample S12.

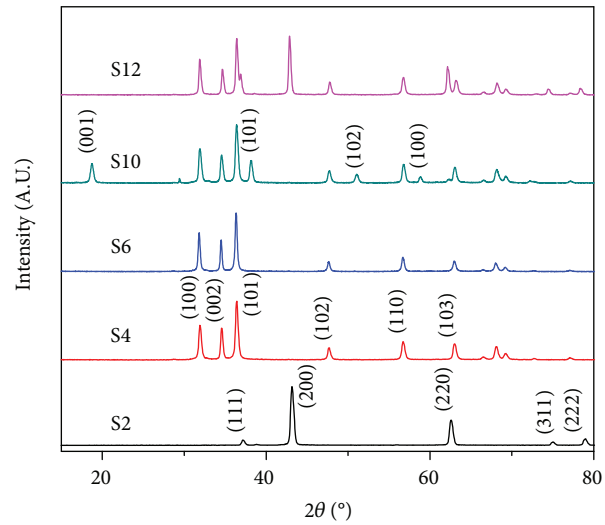

Figure 1: Representative X-ray diffraction patterns of the synthesized nanoparticles. The samples are in agreement with the Joint Committee on Powder Diffraction Standards (JCPDS) reference pattern numbers 00-087-0653 (MgO, periclase), 00-036-1451 (ZnO, zincite), and 00-007-0239 ($Mg(OH)_2$, brucite).

Table 2: Determination of the crystallite size, the average diameter, and MICs of different nanoparticle samples on *Colletotrichum gloeosporioides* obtained from papaya (PG-16) and avocado (AP-14).

Samples	Crystallite size (nm)	Average diameter (nm)	*C. gloeosporioides* MICs (mg/mL)	
			PG-16	AP-14
S1	13	52 ± 18	0.156	0.312
S2	24	96 ± 33	0.312	0.312
S3	22	51 ± 13	0.156	0.312
S4	26	53 ± 17	0.156	0.312
S5	24	63 ± 18	0.312	0.312
S6	37	77 ± 31	0.312	0.312
S7	ZnO NM $Mg(OH)_2$ 23	54 ± 17	0.156	0.312
S8	ZnO NM $Mg(OH)_2$ 30	88 ± 30	0.312	0.312
S9	ZnO NM $Mg(OH)_2$ 23	71 ± 22	0.312	0.312
S10	ZnO NM $Mg(OH)_2$ 24	98 ± 41	0.312	0.312
S11	ZnO 49 MgO 23	139 ± 49	0.312	0.312
S12	ZnO 49 Mg 25	161 ± 44	0.312	0.312
S13	ZnO NM MgO 24	219 ± 39	0.625	0.625

NM: not measured.

3.2. Antifungal Effect of Nanoparticles on Colletotrichum gloeosporioides. The crystallite size (Table 2) of MgO and ZnO synthesized by coprecipitation method at two

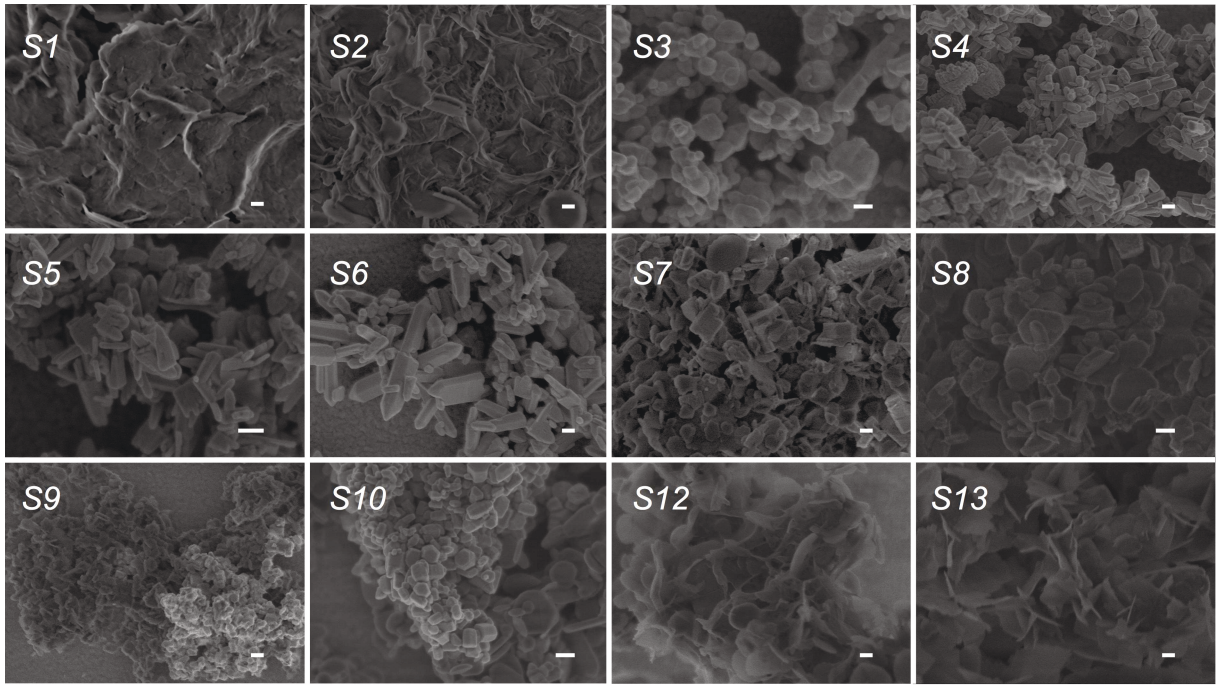

Figure 2: Scanning electron microscopy images of the different synthesized metal oxide nanoparticles. Scale bars correspond to 100 nm for all images.

temperatures was determined using (1) and increases at higher temperature of calcination. The same behavior was observed for ZnO synthesized by hydrothermal method. In the latter case, the pressure inside the vessel contributed to the growth of the crystallites. In the case of ZnO observed in ZnO/$Mg(OH)_2$ composite material, the crystallite size was not determined by the Scherrer equation (1), because the sizes of the crystallites were much larger than 50 nm [27]. Meanwhile, for $Mg(OH)_2$, the size was nearly the same at all treatment temperatures. Finally, the crystallite size of MgO formed in ZnO/MgO composite obtained by coprecipitation method did not change as the calcination temperature increased, although for ZnO, it increases as the calcination temperature is higher, as mentioned earlier.

The average diameter of the particles was also measured (Table 2). The average size and size dispersion of ZnO NPs formed by the coprecipitation method were smaller than those formed by the hydrothermal method. According to the Scherrer approximation, the ZnO crystallite particles had an average diameter larger than 70 nm.

3.2.1. Broth Microdilution Method. In all assay, the MICs were equal to the MFCs, indicating that the action of the NPs was fungicidal. The MICs of MgO NPs (S1 and S2) against *C. gloeosporioides* from papaya increased as the crystallite size grows, although this effect was not observed for the fungus obtained from avocado. The ZnO NPs synthesized by both coprecipitation and hydrothermal methods had similar crystallite sizes; however, slight differences in the generated particle sizes (i.e., smaller sizes) could be related with the lowest MICs against papaya fungi, which corresponded with samples S3, S4, and S7. In the case of the composite NPs, it is difficult to compare the crystallites because they were larger than 50 nm; therefore, the Scherrer equation was not valid [27]. However, particles within the range of 60–161 nm had the same MIC against both fungal strains (0.312 mg/mL). For particles larger than 200 nm, the values of MIC are twice, as observed in sample S13.

With respect to the antifungal activity of the NPs against the *C. gloeosporioides* strains isolated from papaya (PG-16) and avocado (AP-14), we found that a MIC of 0.312 mg/mL was required to totally inhibit strain AP-14, independently of the type of NP (Table 2). The NPs with the lowest MICs against PG-16 were S1, S3, S4, and S7 (0.156 mg/mL); in these latter samples, the size of NPs fluctuated between 51 and 54 nm. With these results, we infer that the smaller NPs have greater antifungal activity and inhibit the germination of the evaluated fungal strains to a greater extent.

3.2.2. Effect of Nanoparticles on Mycelial Radial Growth. The NPs were assayed in culture media with the evaluated strains of *C. gloeosporioides* to test their antifungal activity. The percentages of radial inhibition of the evaluated fungal strains were calculated to understand the antagonistic effects of the NPs on these fungi (Figure 3). Pure ZnO (S3–S6) most actively inhibited both strains of fungi and resulted in percentages of inhibition greater than 80%. Conversely, the MgO NPs as well as the ZnO/MgO and ZnO/$Mg(OH)_2$ composites were the least effective against the fungi, as the presence of Mg had an antagonistic effect on the activity of the ZnO NPs (Figure 4). These results were similar to those reported for the activity of silver NPs against *C. gloeosporioides* from papaya at lower concentrations [9]. Silver NPs can have a higher antimicrobial activity than zinc but have been shown to be toxic in some cases [28]; in addition, zinc oxide NPs can also be used as nutrients by plants [29].

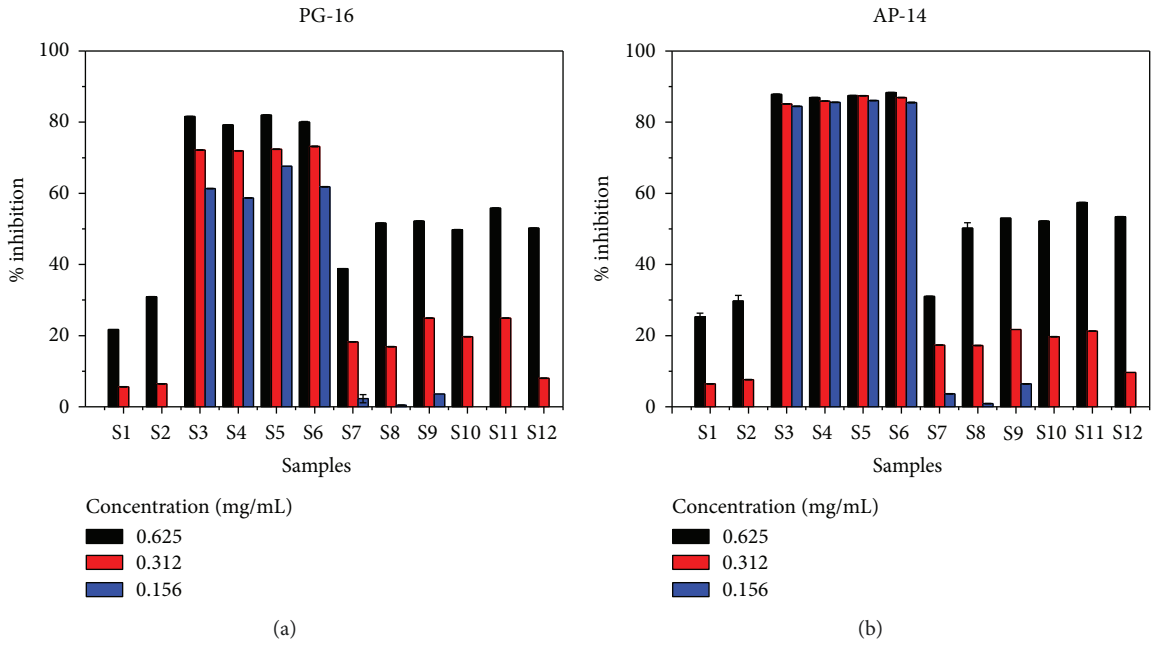

Figure 3: Antifungal activity against two strains of *C. gloeosporioides* of three different concentrations of nanoparticles.

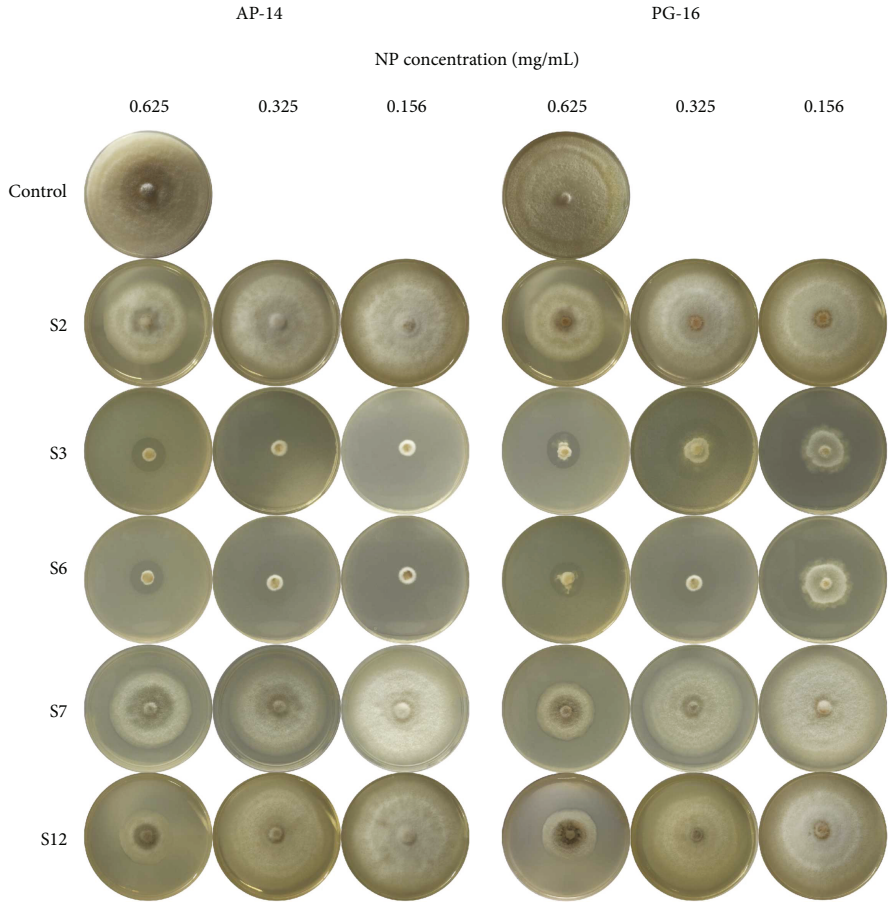

Figure 4: Radial growth inhibition of strains AP-14 and PG-16, by different concentrations of nanoparticles. The synthesis parameters of each image are described in Table 1.

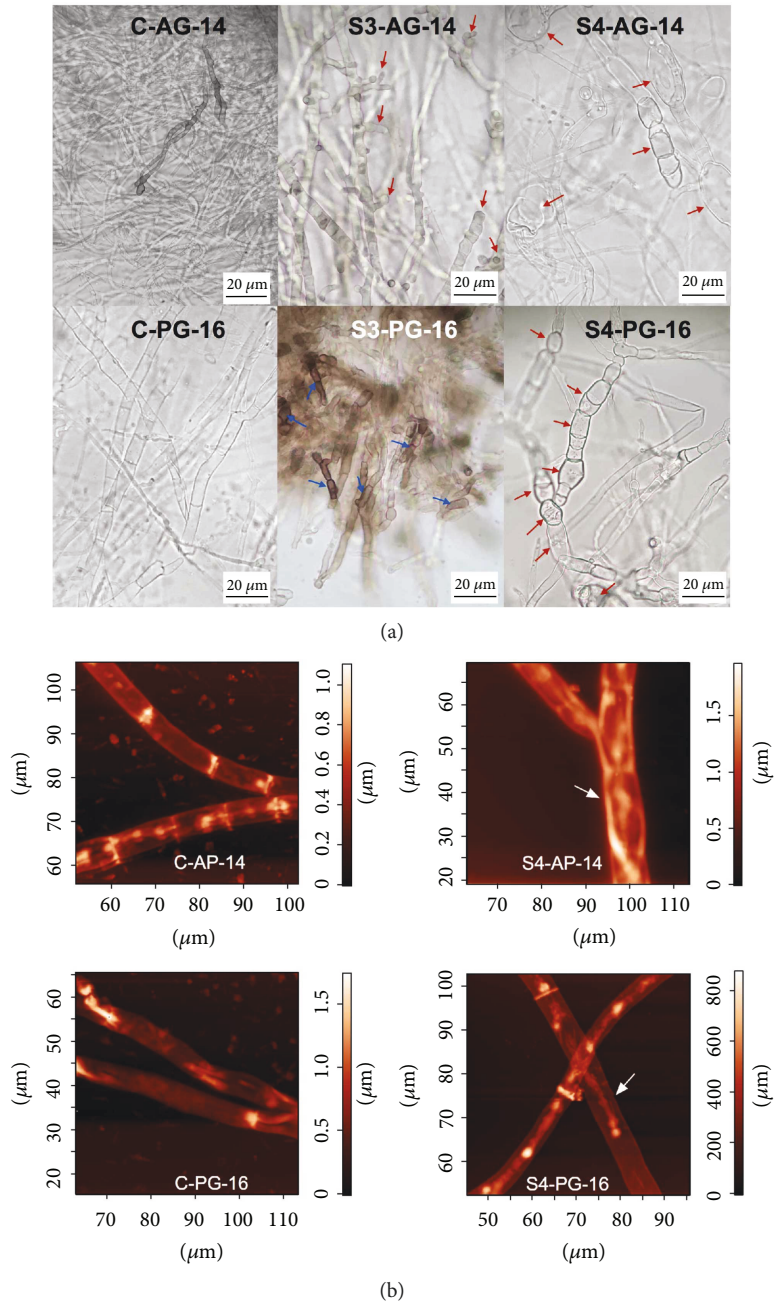

Figure 5: Deformation and structural changes were observed by optical (a) and atomic force microscopy (b). In both strains, the controls with normal hyphae without alterations (C-AG-14 and C-PG-16) are shown, while hyphae swallowed (red and white arrows) and melanization (blue arrows) were caused by the S4 and S3 nanoparticles, respectively.

The radial growth of the fungal strain from papaya (versus avocado) was the least inhibited by the NPs. These results were confirmed by a susceptibility test carried out with commercial antifungal agents (benomyl and prochloraz) in the positive controls of anthracnose strains obtained from avocado and papaya. In both trials, the strain from papaya was more resistant to benomyl than the strain from avocado; the strains from papaya and avocado had MICs of 0.625 and 0.312 μg/mL, respectively. Although, 10 μg/mL of benomyl was necessary to reach 80% and 85% growth inhibition of the strains, from papaya and avocado, respectively. The behavior of prochloraz was similar; the MICs for the strains from papaya and avocado were 0.05 and 0.025 μg/mL, respectively. In this case, only 1 μg/mL of prochloraz was necessary to achieve the total inhibition of both fungi.

Benomyl and prochloraz are effective fungicides for the inhibition of *Colletotrichum* strains that cause anthracnose and other symptoms in several tropical fruits; diverse studies have shown that *Colletotrichum* strains could present

resistance to these compounds [30, 31]. In this study, we found that both evaluated fungal strains showed resistance to 1 μg/mL of benomyl.

Several studies have also examined the interaction of NPs with bacteria [11, 13, 32, 33], although few have examined the effects of NPs on fungi [9, 12, 34]. This may be due to the simplicity of bacterial systems in comparison to fungal systems. Some studies have demonstrated that smaller ZnO particles have greater activity on different kinds of bacteria [32, 35]. In our study, we observed a similar behavior of ZnO NPs on fungi; nevertheless, not all biological systems exhibit similar behavior under the influence of the same external agent.

Notably, Lipovsky and collaborators provided one explanation on the action of ZnO NPs as a fungicide against *Candida albicans* [36]. These researchers found a correlation between ZnO NPs and reactive oxygen species (ROS) that induce cell injury. Also, these researchers reported in a previous work that ZnO NPs are capable of producing ROS in water suspensions [32].

Finally, in the radial growth test, different concentrations of NPs inhibited sporulation or caused deformation by swelling the spores of both strains of *C. gloeosporioides*. In addition, structural deformation and melanization to the hyphae of fungi were observed (Figure 5), as the NPs resulted in the deformation of the hyphae via swelling or vacuolar expansion. Consequently, fungal growth was generally inhibited. Structural damage caused by NPs to other pathogens has been reported by other authors who have found levels of cellular damage similar to those in this study [37–39].

4. Conclusions

Of the synthesized NPs, ZnO obtained by both methods of synthesis (hydrothermal and coprecipitation) demonstrated greater antifungal activity against the two analyzed strains of *C. gloeosporioides* that cause anthracnose in avocado and papaya. The microdilution technique was used to confirm that NP concentrations between 0.156 and 0.625 mg/mL inhibited the spore germination of *C. gloeosporioides* according to the measurement of radial growth and also caused hyphal deformation. In all experiments, the MICs were equal to the MFCs, indicating that the action of the NPs was fungicidal.

However, regardless of the mechanism of action, ZnO NPs can be effective fungicides against *C. gloeosporioides* strains obtained from papaya and avocado. In addition, ZnO NPs may offer additional benefits to plants. The fungal strain from papaya exhibited greater resistance to the evaluated NPs; in contrast, the strain from avocado was more susceptible to the action of the NPs.

Traditional fungicidal treatments to control *C. gloeosporioides* are expensive, and *C. gloeosporioides* presents resistance to some treatments. In this context, NPs represent one alternative for controlling anthracnose caused by *C. gloeosporioides* and can also provide additional nutrients to plants.

Data Availability

All data generated or analyzed during this study are presented in the article and are available from the corresponding author on reasonable request.

Conflicts of Interest

The authors declare no conflict of interest.

Acknowledgments

The authors would like to thank D. Aguilar at LANNBIO (CINVESTAV, Mérida) for the technical assistance in XRD analyses. This work was partially funded by CONACYT Fronteras de la Ciencia (Project Code no. 138) and Consejo de la Investigacion Cientifica, Universidad Michoacana de San Nicolás de Hidalgo (UMSNH), Research Project 2017.

References

[1] S. Freeman, T. Katan, and E. Shabi, "Characterization of *Colletotrichum gloeosporioides* isolates from avocado and almond fruits with molecular and pathogenicity tests," *Applied and Environmental Microbiology*, vol. 62, no. 3, pp. 1014–1020, 1996.

[2] G. Huerta-Palacios, F. Holguín-Meléndez, F. A. Benítes-Camilo, and J. Toledo-Arreola, "Epidemiología de la Antracnosis (*Colletotrichum gloeosporioides* (Penz.) Penz. and Sacc.) en el Mango (*Magnifera indica* L.) cv. Ataulfo en el Soconusco Chiapas, Mexico," *Revista Mexicana de Fitopatologia*, vol. 27, pp. 93–105, 2009.

[3] M. Sharma and S. Kulshrestha, "*Colletotrichum gloeosporioides*: an anthracnose causing pathogen of fruits and vegetables," *Biosciences Biotechnology Research Asia*, vol. 12, no. 2, pp. 1233–1246, 2015.

[4] S. Bautista-Baños, *Postharvest Decay: Control Strategies*, Elsevier, 2014.

[5] G. Sharma, M. Maymon, and S. Freeman, "Epidemiology, pathology and identification of *Colletotrichum* including a novel species associated with avocado (*Persea americana*) anthracnose in Israel," *Scientific Reports*, vol. 7, no. 1, article 15839, 2017.

[6] S. W. Kim, K. S. Kim, K. Lamsal et al., "An *in vitro* study of the antifungal effect of silver nanoparticles on oak wilt pathogen *Raffaelea* sp," *Journal of Microbiology and Biotechnology*, vol. 19, no. 8, pp. 760–764, 2009.

[7] H. Ishii and D. W. Hollomon, *Fungicide Resistance in Plant Pathogens: Principles and a Guide to Practical Management*, Springer, 2015.

[8] P. Del Serrone, M. Nicoletti, and L. Buttazzoni, "Nutrition and multiresistence alert," *EC Nutrition*, vol. 4, pp. 772–783, 2016.

[9] M. A. Aguilar-Méndez, E. San Martín-Martínez, L. Ortega-Arroyo, G. Cobián-Portillo, and E. Sánchez-Espíndola, "Synthesis and characterization of silver nanoparticles: effect on phytopathogen *Colletotrichum gloesporioides*," *Journal of Nanoparticle Research*, vol. 13, no. 6, pp. 2525–2532, 2011.

[10] S. M. Ali, N. M. H. Yousef, and N. A. Nafady, "Application of biosynthesized silver nanoparticles for the control of land snail *Eobania vermiculata* and some plant pathogenic fungi,"

Journal of Nanomaterials, vol. 2015, Article ID 218904, 10 pages, 2015.

[11] E. Alzahrani and R. A. Ahmed, "Synthesis of copper nanoparticles with various sizes and shapes: application as a superior non-enzymatic sensor and antibacterial agent," *International Journal of Electrochemical Science*, vol. 11, pp. 4712–4723, 2016.

[12] K. Bramhanwade, S. Shende, S. Bonde, A. Gade, and M. Rai, "Fungicidal activity of Cu nanoparticles against *Fusarium* causing crop diseases," *Environmental Chemistry Letters*, vol. 14, no. 2, pp. 229–235, 2016.

[13] G. R. Navale, D. J. Late, and S. S. Shinde, "Antimicrobial activity of ZnO nanoparticles against pathogenic bacteria and fungi," *JSM Nanotechnology & Nanomedicine*, vol. 3, 2015.

[14] J. Panigrahi, D. Behera, I. Mohanty, U. Subudhi, B. B. Nayak, and B. S. Acharya, "Radio frequency plasma enhanced chemical vapor based ZnO thin film deposition on glass substrate: a novel approach towards antibacterial agent," *Applied Surface Science*, vol. 258, no. 1, pp. 304–311, 2011.

[15] A. J. Fonseca, F. Pina, M. F. Macedo et al., "Anatase as an alternative application for preventing biodeterioration of mortars: evaluation and comparison with other biocides," *International Biodeterioration & Biodegradation*, vol. 64, no. 5, pp. 388–396, 2010.

[16] L. P. Zheng, Z. Zhang, B. Zhang, and J. W. Wang, "Antifungal properties of Ag-SiO_2 core-shell nanoparticles against phytopathogenic fungi," *Advanced Materials Research*, vol. 476-478, pp. 814–818, 2012.

[17] J. M. Köhler, L. Abahmane, J. Wagner, J. Albert, and G. Mayer, "Preparation of metal nanoparticles with varied composition for catalytical applications in microreactors," *Chemical Engineering Science*, vol. 63, no. 20, pp. 5048–5055, 2008.

[18] B. J. Perelaer, A. W. M. de Laat, C. E. Hendriks, and U. S. Schubert, "Inkjet-printed silver tracks: low temperature curing and thermal stability investigation," *Journal of Materials Chemistry*, vol. 18, no. 27, p. 3209, 2008.

[19] L. M. Bronstein, D. M. Chernyshov, I. O. Volkov et al., "Structure and properties of bimetallic colloids formed in polystyrene-*block*-poly-4-vinylpyridine micelles: catalytic behavior in selective hydrogenation of dehydrolinalool," *Journal of Catalysis*, vol. 196, no. 2, pp. 302–314, 2000.

[20] J. Tomas, "Mechanics of nanoparticle adhesion — a continuum approach," *Particles on Surfaces 8: Detection, Adhesion and Removal*, pp. 1–47, 2003.

[21] N. M. Gómez-Ortíz, W. S. González-Gómez, S. C. de la Rosa-García et al., "Antifungal activity of $Ca[Zn(OH)_3]_2{\cdot}2H_2O$ coatings for the preservation of limestone monuments: an *in vitro* study," *International Biodeterioration & Biodegradation*, vol. 91, pp. 1–8, 2014.

[22] P. Tamilselvi, A. Yelilarasi, M. Hema, and R. Anbarasan, "Synthesis of hierarchical structured MgO by sol gel method," *Nano Bulletin*, vol. 2, article 1301061, 2013.

[23] B. C. Sutton, *The Coelomycetes. Fungi Imperfecti with Pycnidia, Acervuli and Stromata*, CMI, Kew, 1980.

[24] B. S. Weir, P. R. Johnston, and U. Damm, "The *Colletotrichum gloeosporioides* species complex," *Studies in Mycology*, vol. 73, no. 1, pp. 115–180, 2012.

[25] J. M. Andrews, "Determination of minimum inhibitory concentrations," *The Journal of Antimicrobial Chemotherapy*, vol. 48, Supplement 1, pp. 5–16, 2001.

[26] D. K. Pandey, N. N. Tripathi, R. D. Tripathi, and S. Dixit, "Fungitoxic and phytotoxic properties of the essential oil of *Hyptis suaveolens*," *Journal of Plant Diseases and Protection*, vol. 89, pp. 344–349, 1982.

[27] J. I. Langford and A. J. C. Wilson, "Scherrer after sixty years: a survey and some new results in the determination of crystallite size," *Journal of Applied Crystallography*, vol. 11, no. 2, pp. 102–113, 1978.

[28] C. Beer, R. Foldbjerg, Y. Hayashi, D. S. Sutherland, and H. Autrup, "Toxicity of silver nanoparticles-nanoparticle or silver ion?," *Toxicology Letters*, vol. 208, no. 3, pp. 286–292, 2012.

[29] J. R. Peralta-Videa, J. A. Hernandez-Viezcas, L. Zhao et al., "Cerium dioxide and zinc oxide nanoparticles alter the nutritional value of soil cultivated soybean plants," *Plant Physiology and Biochemistry*, vol. 80, pp. 128–135, 2014.

[30] G. M. Sanders, L. Korsten, and F. C. Wehner, "Market survey of post-harvest diseases and incidence of *Colletotrichum gloeosporioides* on avocado and mango fruit in South Africa," *Tropical Science*, vol. 40, pp. 192–198, 2000.

[31] X. F. Xu, T. Lin, S. K. Yuan et al., "Characterization of baseline sensitivity and resistance risk of *Colletotrichum gloeosporioides* complex isolates from strawberry and grape to two demethylation-inhibitor fungicides, prochloraz and tebuconazole," *Australasian Plant Pathology*, vol. 43, no. 6, pp. 605–613, 2014.

[32] G. Applerot, A. Lipovsky, R. Dror et al., "Enhanced antibacterial activity of nanocrystalline ZnO due to increased ROS-mediated cell injury," *Advanced Functional Materials*, vol. 19, no. 6, pp. 842–852, 2009.

[33] I. Perelshtein, A. Lipovsky, N. Perkas, A. Gedanken, E. Moschini, and P. Mantecca, "The influence of the crystalline nature of nano-metal oxides on their antibacterial and toxicity properties," *Nano Research*, vol. 8, no. 2, pp. 695–707, 2015.

[34] A. H. Wani and M. A. Shah, "A unique and profound effect of MgO and ZnO nanoparticles on some plant pathogenic fungi," *Journal of Applied Pharmaceutical Science*, vol. 2, pp. 40–44, 2012.

[35] O. Yamamoto, "Influence of particle size on the antibacterial activity of zinc oxide," *International Journal of Inorganic Materials*, vol. 3, no. 7, pp. 643–646, 2001.

[36] A. Lipovsky, Y. Nitzan, A. Gedanken, and R. Lubart, "Antifungal activity of ZnO nanoparticles—the role of ROS mediated cell injury," *Nanotechnology*, vol. 22, no. 10, article 105101, 2011.

[37] L. He, Y. Liu, A. Mustapha, and M. Lin, "Antifungal activity of zinc oxide nanoparticles against *Botrytis cinerea* and *Penicillium expansum*," *Microbiological Research*, vol. 166, no. 3, pp. 207–215, 2011.

[38] K. Kairyte, A. Kadys, and Z. Luksiene, "Antibacterial and antifungal activity of photoactivated ZnO nanoparticles in suspension," *Journal of Photochemistry and Photobiology B: Biology*, vol. 128, pp. 78–84, 2013.

[39] A. Król, P. Pomastowski, K. Rafińska, V. Railean-Plugaru, and B. Buszewski, "Zinc oxide nanoparticles: synthesis, antiseptic activity and toxicity mechanism," *Advances in Colloid and Interface Science*, vol. 249, pp. 37–52, 2017.